JOC The Journal of Organic Chemistry

Article

pubs.acs.org/joc

Chiroptical Studies on Brevianamide B: Vibrational and Electronic Circular Dichroism Confronted

Patrick Bultinck,[†,‡] Fanny L. Cherblanc,[§] Matthew J. Fuchter,[*,§] Wouter A. Herrebout,[‡,∥] Ya-Pei Lo,[§] Henry S. Rzepa,[*,§] Giuliano Siligardi,[⊥] and Marko Weimar[§]

[†]Department of Inorganic and Physical Chemistry, Ghent University, Krijgslaan 281 S3, B9000 Ghent, Belgium

[‡]European Centre for Chirality, Krijgslaan 281 S3, B9000 Ghent, Belgium

[§]Department of Chemistry, Imperial College London South Kensington Campus, London SW7 2AZ, United Kingdom

[∥]Department of Chemistry, University of Antwerp Groenenborgerlaan 171, 2020 Antwerp, Belgium

[⊥]Diamond Light Source, Chilton, Oxon OX11 0QX, United Kingdom

Supporting Information

ABSTRACT: Chiroptical spectroscopies, such as electronic circular dichroism (ECD) and vibrational circular dichroism (VCD), are highly sensitive techniques to probe molecular conformation, configuration, solvation, and aggregation. Here we report the application of these techniques to study the fungal metabolite brevianamide B. Comparison of the experimental ECD and VCD spectra with the density functional theory simulated counterparts establishes that VCD is the more reliable technique to assign absolute configuration due to the larger functional and dispersion dependence of computed ECD spectra. Despite a low amount of available material and a relatively unusual example of using VCD carbonyl multiplets, the absolute configuration could be reliably predicted, strengthening the case for application of VCD in the study of complex natural products. Spectral and crystallographic evidence for or against the formation of a dimeric aggregate is discussed; in solution, the VCD spectra strongly suggest only monomeric species are present.

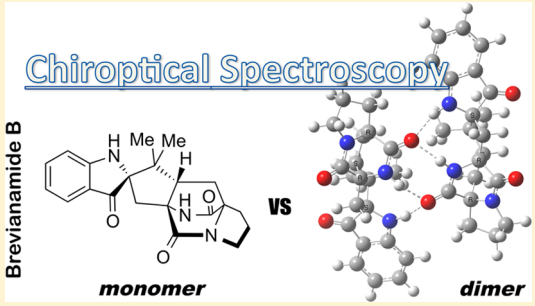

INTRODUCTION

Chiroptical spectroscopy uses refraction, absorption, or emission of anisotropic radiation to probe the dissymmetry of a substance. Such spectroscopic techniques include optical rotation at a fixed wavelength, optical rotatory dispersion (ORD), and electronic circular dichroism (ECD), which are associated with electronic transitions,[1] as well as the more recent techniques of vibrational circular dichroism (VCD) and Raman optical activity (ROA), which focus on vibrational transitions.[2] Importantly, these techniques are powerful tools to elucidate molecular conformation, configuration, solvation, and aggregation.[3,4] We have recently reported the use of comparative chiroptical studies, comparing experimentally obtained spectra with theoretical simulations, to elucidate the stereochemistry of a desulfurized derivative of the fungal epipolythiodioxopiperazine (ETP) metabolite chaetocin.[5] Driven by a mechanistic hypothesis, we also discovered stereochemical misassignments of a related ETP natural product analogue dethiodehydrogliotoxin,[5] as well as a synthetic ETP analogue.[6] Before the advent of both experimental setups and computational tools for the more or less routine assignment of absolute configurations, it was common practice to use correlative methods to assign stereochemistry. This means that one assumed that similar chromophore frameworks would possess similar spectra. Especially in ECD, this has been (and to some degree continues to be) a fairly standard approach. It is only relatively recently that computational power and new algorithms for the ab initio prediction of spectra have enabled suitably accurate quantum-chemical simulations of the chiroptical spectra of larger molecules to allow unambiguous comparison. In light of the questionable validity of the correlative methods[7] used to assign the absolute stereochemistry of several diketopiperazines (such as dethiodehydrogliotoxin[5,6]), we undertook a study of other natural product frameworks bearing substituted diketopiperazines.

The brevianamides comprise an interesting family of indole alkaloids.[8] (+)-Brevianamide A (**1**) was originally isolated from *Penicillium brevicompactum* in 1969,[9] with further brevianamides later isolated.[10] The structure and absolute stereochemistry of brevianamide A (**1**) was established using X-ray crystallography of a semisynthetic brominated derivative.[11] Determination of the structure and absolute stereochemistry of the minor metabolite brevianamide B (**3**), on the other hand, was more complex. The original structure was inferred from semisynthetic reduction of brevianamide A (**1**) to deoxybrevianamide (**2**), followed by stereoselective oxidation to give (−)-brevianamide B (**3**, Scheme 1).[10] This structure and the proposed absolute

Received: October 3, 2014
Published: March 3, 2015

DOI: 10.1021/jo5022647
J. Org. Chem. 2015, 80, 3359−3367

Scheme 1

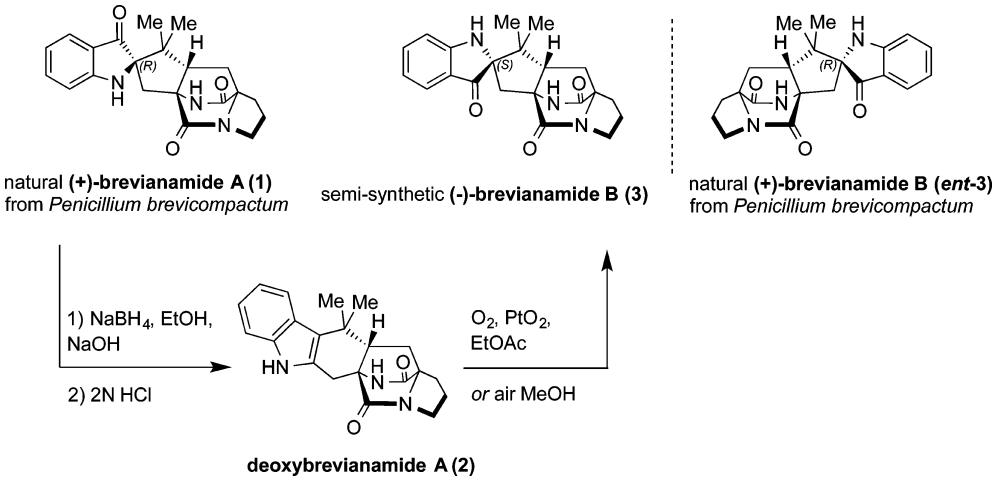

stereochemistry were later confirmed by Williams and co-workers using total synthesis.[12] Curiously, however, a chiroptical comparison revealed the naturally occurring (+)-brevianamide B (*ent*-**3**) to be the enantiomorph of the semi- or totally synthetic product **3** (Scheme 1).[13] While such a result has fascinating implications from a biosynthetic standpoint, we decided to revisit the chiroptical spectra of brevianamides A and B to further our study of substituted diketopiperazine stereochemistry using such methods. This paper reports experimentally obtained and theoretically predicted ECD and VCD spectra for both the monomeric form of (−)-brevianamide B, as well as a hypothesized dimer. Not only does this study further highlight the value of chiroptical methods in probing molecular structure, it also represents a highly unusual example of using carbonyl stretch band features in VCD to study complex natural products.[14] Moreover, as will be shown below, brevianamides A and B are excellent examples of the added value of VCD spectroscopy compared to ECD in terms of the calculation of theoretical spectra using density functional theory (DFT) methods.

RESULTS AND DISCUSSION

Since we have previously used highly sensitive chiroptical spectroscopy to probe the stereochemistry and structure of diketopiperazine natural products,[5,6] we decided to employ such techniques to study (−)-brevianamide B (**3**). It should be noted that comparative studies linking different experimental and simulated chiroptical spectra of such large molecular weight, complex natural products are still comparatively rare, hence the present chiroptical study of brevianamide B using ECD and VCD.

ECD spectra have been previously reported for brevianamides A and B.[13] These were recorded in trifluoroethanol (TFE) between 200 and 250 nm and in 2.5% formic acid/dichloromethane (DCM) between 250 and 450 nm. Although ECD spectra can be simulated using ab initio techniques, including a solvent model, these mostly use a continuum representation, and so any explicit hydrogen bonding, as may be expected for a protic cosolvent, is not modeled. Indeed, explicit solvation remains a challenge especially for larger molecules where several (co)solvent molecules would be required that may, moreover, be arranged in many different ways. Since our calculations (vide infra) do not account for explicit solvent interactions, we felt that a comparison between the experimental formic acid/DCM spectra and our computed spectra would be less appropriate. Therefore, using the B23

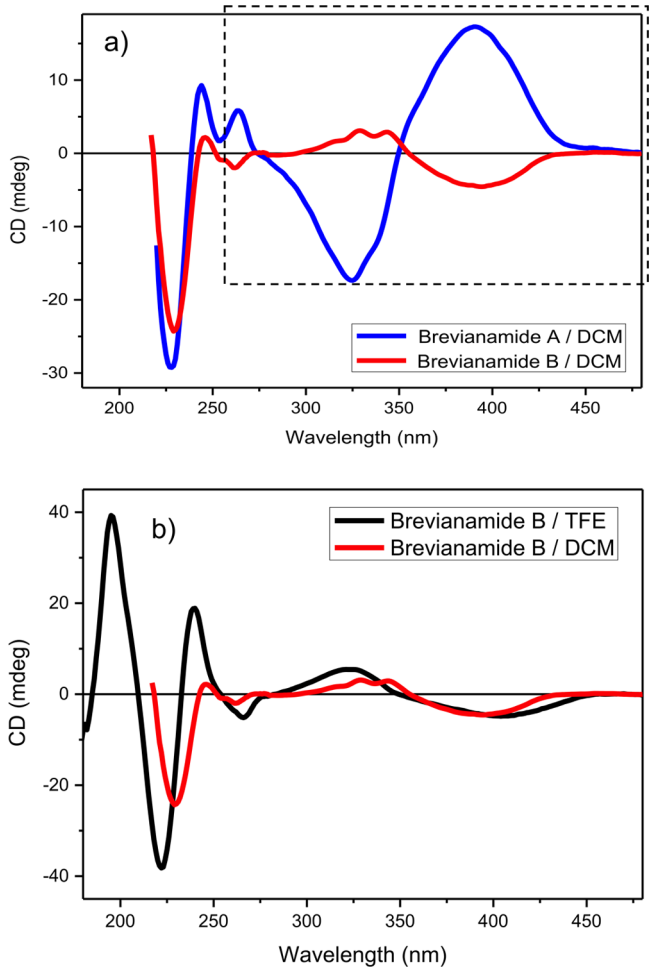

Figure 1. Measured synchrotron radiation ECD (SR-ECD) spectra of brevianamide A and B: (a) comparison of (+)-brevianamide A (**1**) and (−)-brevianamide B (**3**) in DCM; (b) comparison of (−)-brevianamide B in DCM and TFE. The SR-ECD spectra for all solutions were measured in the region below 280 nm with a 1 mm path length and the 280−480 nm region with a 10 mm path length. In both panels, the spectra from 280 to 480 nm were normalized to a 1 mm path length by dividing the data by 10.

DOI: 10.1021/jo5022647
J. Org. Chem. 2015, 80, 3359−3367

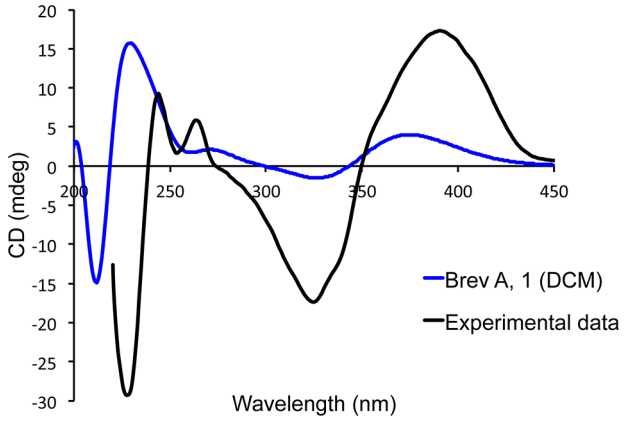

Figure 2. Calculated spectrum of (+)-brevianamide A (**1**) with a continuum solvent field (SCRF) for DCM using M062X/6-311++G(d,p). The calculated ECD curves were shifted by +30 nm and convoluted with a line width of 0.333 eV. The SR-ECD normalized experimental data (Figure 1), measured in DCM, are overlaid for comparison.

circular dichroism beamline at the Diamond Synchrotron Facility, synchrotron radiation (SR)-ECD spectra of samples of brevianamide A (**1**) and semisynthetic (−)-brevianamide B (**3**) could be obtained; in the case of semisynthetic (−)-brevianamide B (**3**), a highly insoluble material. The use of synchrotron radiation makes it possible to measure ECD spectra at significantly lower concentrations due to the better signal-to-noise ratio. This is particularly important for brevianamide B due to its very low solubility in pure DCM (and in a range of organic solvents) as compared to the previously used DCM/formic acid solution. The measured ECD spectra of brevianamide A (**1**) and (−)-brevianamide B (**3**) in DCM are shown in Figure 1, along with a comparison of the ECD spectra of (−)-brevianamide B (**3**) in TFE and DCM.

The obtained ECD spectra (Figure 1) in a single solvent system were in good agreement with those obtained previously.[13] The mirrored ECD bands in the near-UV region (see inset, Figure 1a) are due to the spiroindoxil quaternary center of *R* and *S* configurations for (+)-brevianamide A (**1**) and (−)-brevianamide B (**3**), respectively (see Scheme 1). Conversely, the ECD bands in the far-UV region are consistent with the rest of the brevianamide scaffold that has the same chiral configuration in both **1** and **3**. Interestingly, it was correlative methods involving this latter ECD region, containing the diketopiperzine chromophore, that we previously found to have led to stereochemical misassignments for the ETP class of natural products.[5,6]

With suitable experimental ECD spectra in hand, comparative computational ECD simulations were carried out using Gaussian 09,[15] employing DFT in its Kohn−Sham implementation. In previous studies on diketopiperazine scaffolds, we had surveyed a range of functionals and basis sets for such calculations[5] and had found that the M062X[6] functional generally gave the best predictions to allow comparison with experimentally obtained spectra. Our new calculations were

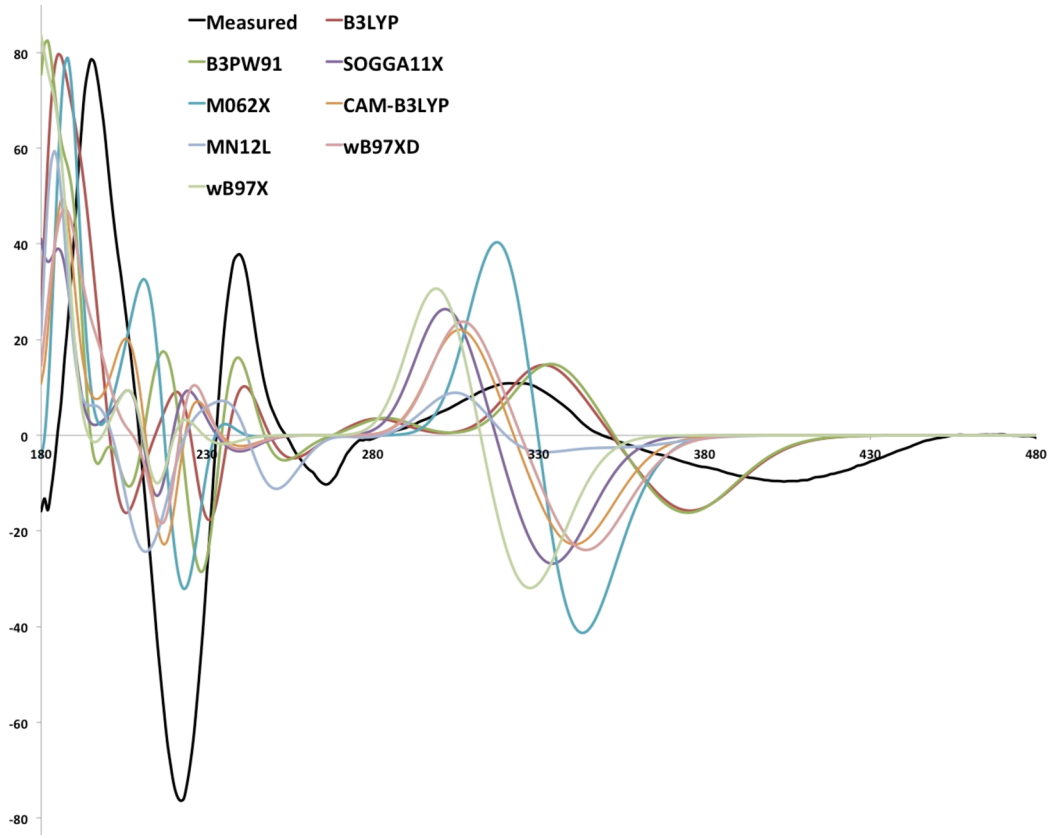

Figure 3. Calculated spectra of (−)-brevianamide B (**3**) with a continuum solvent field (SCRF) for TFE, using a range of functionals and the 6-311++G(d,p) basis set. The calculated ECD curves were unshifted and convoluted with a line width of 0.15 eV. The normalized SR-ECD experimental data (Figure 1), measured in TFE, are overlaid for comparison (black curve). Individual traces can be accessed via the spreadsheet provided with the Supporting Information.

DOI: 10.1021/jo5022647
J. Org. Chem. 2015, 80, 3359−3367

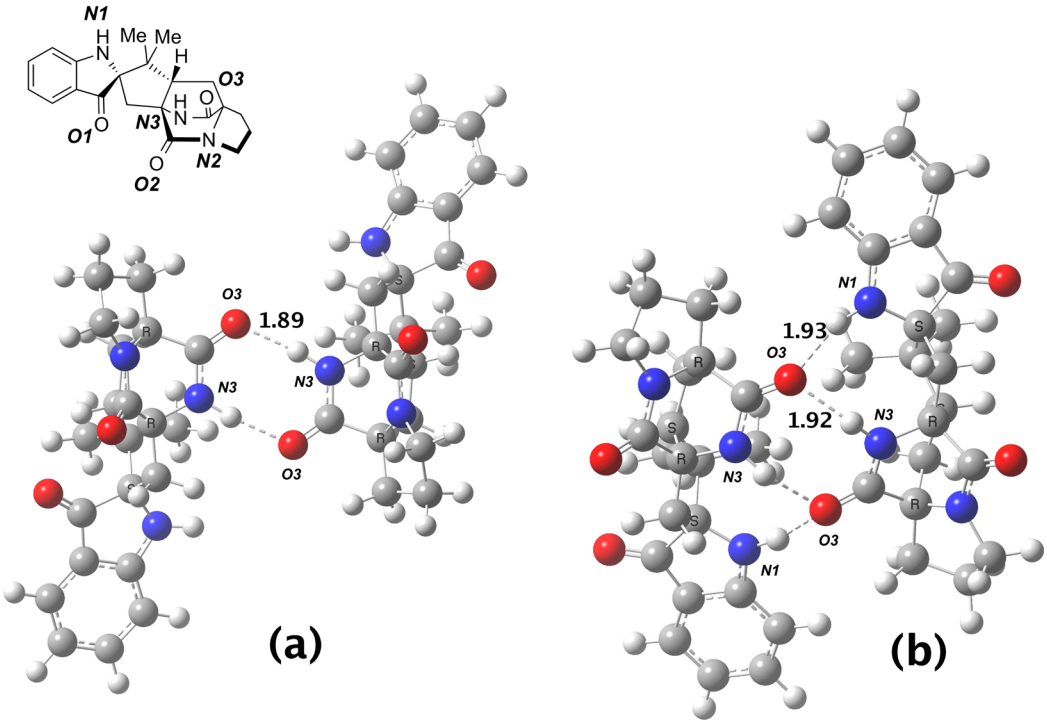

Figure 4. Computed geometry of a proposed C_2-symmetric dimer (**4**) of (−)-brevianamide B using (a) B3LYP/6-311++G(d,p) with a continuum solvent field (SCRF) for TFE and (b) with inclusion of D3 dispersion.[17] Numerical values of bond lengths are in Å. Select heteroatoms have been numbered to facilitate inspection of these structures. Interactive models of these structures can be inspected in WEO1 in the HTML version of this article and where links to the digital repository entries for each calculation can be found.

modified from the original procedures[5] to increase significantly the number of states computed for the time-dependent DFT (TDDFT) from 50 to 100 previously to 250. It is known[16] that the 200−250 nm region can be poorly converged in terms of band shape if insufficient states are considered. The greater number of states also induces a ∼4-fold increase in computation time and, in combination with the basis set, represents a practical upper limit to what can be simulated with current computer resources (64 processors, 90 GB memory) for molecules of the size of **4**.

The simulated spectrum of brevianamide A (**1**) using the 6-311++G(d,p) basis set and the M062X functional gave reasonably good agreement with the experimental spectrum, correctly predicting the positive and negative features, albeit with relative intensities that are not very well predicted (Figure 2).

When we repeated this procedure for brevianamide B, the match to experiment using this functional was far less good (as opposed to the good performance in previous cases of diketopiperazine natural products[5,6]), and we therefore repeated our scan of functionals for this system (Figure 3), albeit with a change of continuum solvent to 2,2,2-trifluoroethanol to allow comparison with the richer experimental data (Figure 1b).

These simulations reveal that no uniform baseline shift (or line width) can be applied that would bring the entire spectral range into good agreement with the experimental data for any of these functionals, and we therefore decided against trying to apply any such corrections as an aid to our interpretations. Although the agreement with experiment for all these functionals might be good enough as evidence to assign the absolute configuration of the species, the changes between the different spectra are significant. Moreover, we wished to explore whether more subtle features of this structure such as aggregation might be revealed by the ECD technique. For example, upon careful consideration of the three-dimensional structure of (−)-brevianamide B (**3**), we hypothesized that formation of a hydrogen-bonded brevianamide B dimer **4** may be possible (Figure 4). We note that the stereochemistry of brevianamide A would prevent it from forming a comparable dimer.

The hydrogen-bonding network shown Figure 4, and particularly the bifurcated form (Figure 4b), has ample precedent in the Cambridge crystal database.[18] There are 376 examples containing such hydrogen bonds (shown as dashed lines in the figure) for which all four recorded lengths are <2.0 Å (see the Supporting Information for individual examples). These have the potential of providing suitably strong interactions to ensure that the proposed molecular dimer is retained in solution, although we do recognize that the range of concentrations and temperatures where ECD is usually recorded normally mitigates against dimer formation. A further note of caution was generated from the computed free energy ΔG_{298} of a monomer−dimer (**3**/**4**) equilibrium in TFE, favoring the monomer by 3.1 kcal/mol (M062X/6-311++g(d,p)/SCRF=TFE) for a standard state of 0.041 M. However, this difference is not so large as to definitively exclude the possibility of a significant concentration of dimer **4** in solution.

Since the formation of a molecular dimer would be expected to be concentration-dependent, with high concentrations favoring dimer formation, an ECD spectrum was recorded for brevianamide B (**3**) as a drop-cast thin film, a highly concentrated condensed phase (Figure 5a). Sample rotation about the surface normal revealed that the observed ECD spectrum was not complicated by linear dichroism contribu-

DOI: 10.1021/jo5022647
J. Org. Chem. 2015, 80, 3359−3367

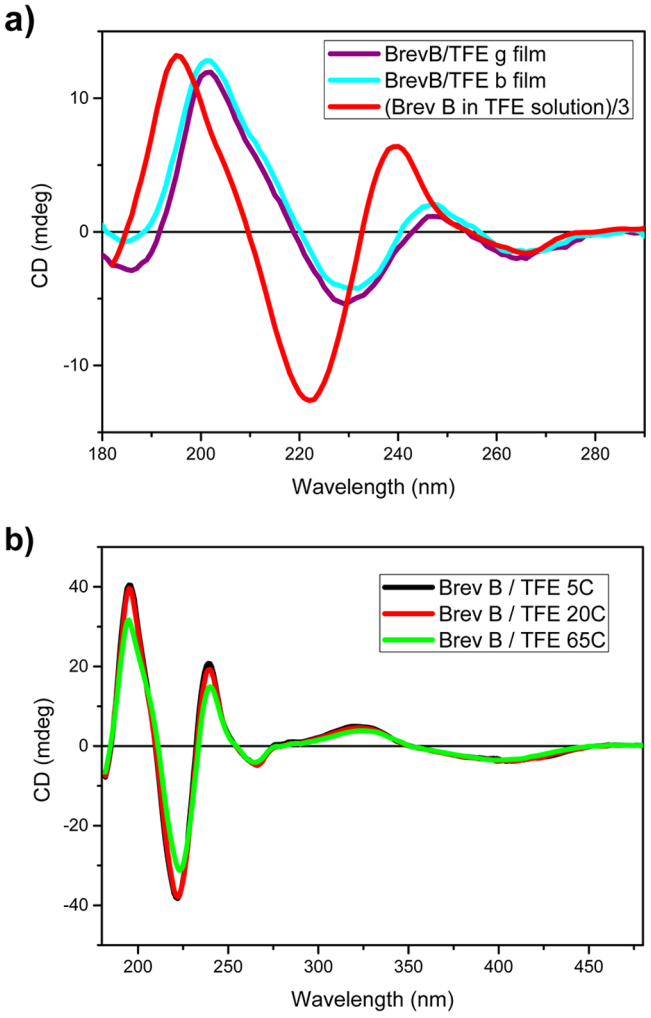

Figure 5. (a) Measured SR-ECD spectra of a brevianamide B thin film (evaporated from TFE) in two perpendicular orientations (g and b) normal to the surface. Normalized solution spectrum included for comparison. (b) Measured SR-ECD spectra of (−)-brevianamide B in TFE at different temperatures. The SR-ECD spectra for all solutions were measured in the region below 280 nm with a 1 mm path length and the 280−480 nm region with a 10 mm path length. In both panels, the spectra from 280 to 480 nm were normalized to a 1 mm path length by dividing the data by 10.

tions. The thin film spectrum qualitatively corresponded to that obtained in dilute solution, albeit red-shifted by about 7 nm. These data suggest that the molecular species in the drop-cast film may be the same as in dilute solution. Concurrently, a temperature study was carried out where an ECD of (−)-brevianamide B in TFE was taken at temperatures ranging from 5 to 65 °C. Should monomer **3** and proposed dimer **4** be in equilibrium in solution, changes in temperature would be expected to perturb this equilibrium, resulting in different ECD spectra. Little or no change was observed in the ECD spectra upon increasing the temperature of the sample (Figure 5b). This suggests that a monomer−dimer equilibrium is not in operation and that the molecular species observed is not sensitive to temperature. Taken together, these data support a single molecular species in solution and in a condensed state and restrict us to consider either a pure monomer distribution or a pure dimer distribution.

At this stage, we decided to evaluate whether an ECD simulation could provide more information about this aspect by asking whether the dimer simulation is perturbed from that of the monomer. There are two broad classes of DFT functionals, as listed in Figure 3, those where no default correction for dispersion terms is included in the functional (B3LYP, B3PW91, CAM-B3LYP) and a second class where such a correction is included (SOGGA11X, M062X, MN12L, ωB97X, ωB97X-D). The optimized geometries for each class differ significantly, suggesting that dispersion has a significant effect on the final structures. The effect is best illustrated by comparing the computed geometry using the B3LYP functional to that obtained when Grimme's D3 functional is added (Figure 4).[17] The B3LYP geometry obtained with the D3 correction now closely matches those obtained from the dispersion-included functionals. The dispersion-corrected predicted dimer structures reveal bifurcation of the hydrogen bonds to the carbonyl groups and a much closer approach of the alkyl groups, as indeed is supported by the crystallographic evidence noted above.

These geometric effects propagate to the predicted ECD dimer spectra (Figure 6a,b), which reveal that, for the functionals without dispersion correction, the effect of dimer formation is reflected only in the intensities of the responses and not their frequencies. We caution against the use of functionals such as the commonly used CAM-B3LYP for exploring the specific property of dimer formation unless they are corrected for dispersion. In contrast, simulated spectra for the dimer-containing bifurcated hydrogen bonds (from dispersion-corrected functionals) additionally show a red shift, ranging from ∼9 nm (M062X) and ∼15 nm (ωB97XD) to ∼40 nm (MN12L) for the lowest energy transitions (Figure 6c,d). It became clear, however, that the variation in the differing functional predictions was still large enough to mask any effects due to any possible aggregation of **3**. There was also a small shift in the 230 nm region between the two possible conformations for the terminal 5-ring present in **3** (see Experimental Section), which adds further noise to any interpretation. Concentrating on a single functional to try to achieve some cancellation of errors, we turned to a more direct comparison with the experimental data. Figure 7 shows the ECD spectra simulated using just the MN12L functional for both solution/gas phase and for monomer/dimer. The experimental data (Figure 5a) shows a red shift of ∼7 nm in the 230 nm region when changing from TFE solution to a solid-state measurement. The MN12L calculations (Figure 7) show a blue shift for the ∼230 nm excitation (+ve Cotton effect) for the monomer solution (233 nm) compared with the monomer gas phase (223 nm) but a smaller blue shift compared with the dimer gas phase (229 nm). Given that the 230 nm region is also where small (∼5 nm) variations due to the conformation adopted by the terminal 5-ring occur, we consider that the evidence for dimer formation in the solid state at best is tenuous, and that for aggregation in solution is even weaker. To seek more conclusive evidence for any possible aggregation of **3** in solution, we turned to vibrational circular dichroism or VCD, an alternative chiroptical technique.

The use of VCD to study the dimerization of molecules in solution is relatively well-known for carboxylic acids,[19] and we note that the bifurcated H-bonded motif shown in Figure 4 for **4** is actually structurally closely related. We therefore assessed the VCD method for both its functional dependence of the monomer spectra and to evaluate the possibility of carboxylic-

DOI: 10.1021/jo5022647
J. Org. Chem. 2015, 80, 3359−3367

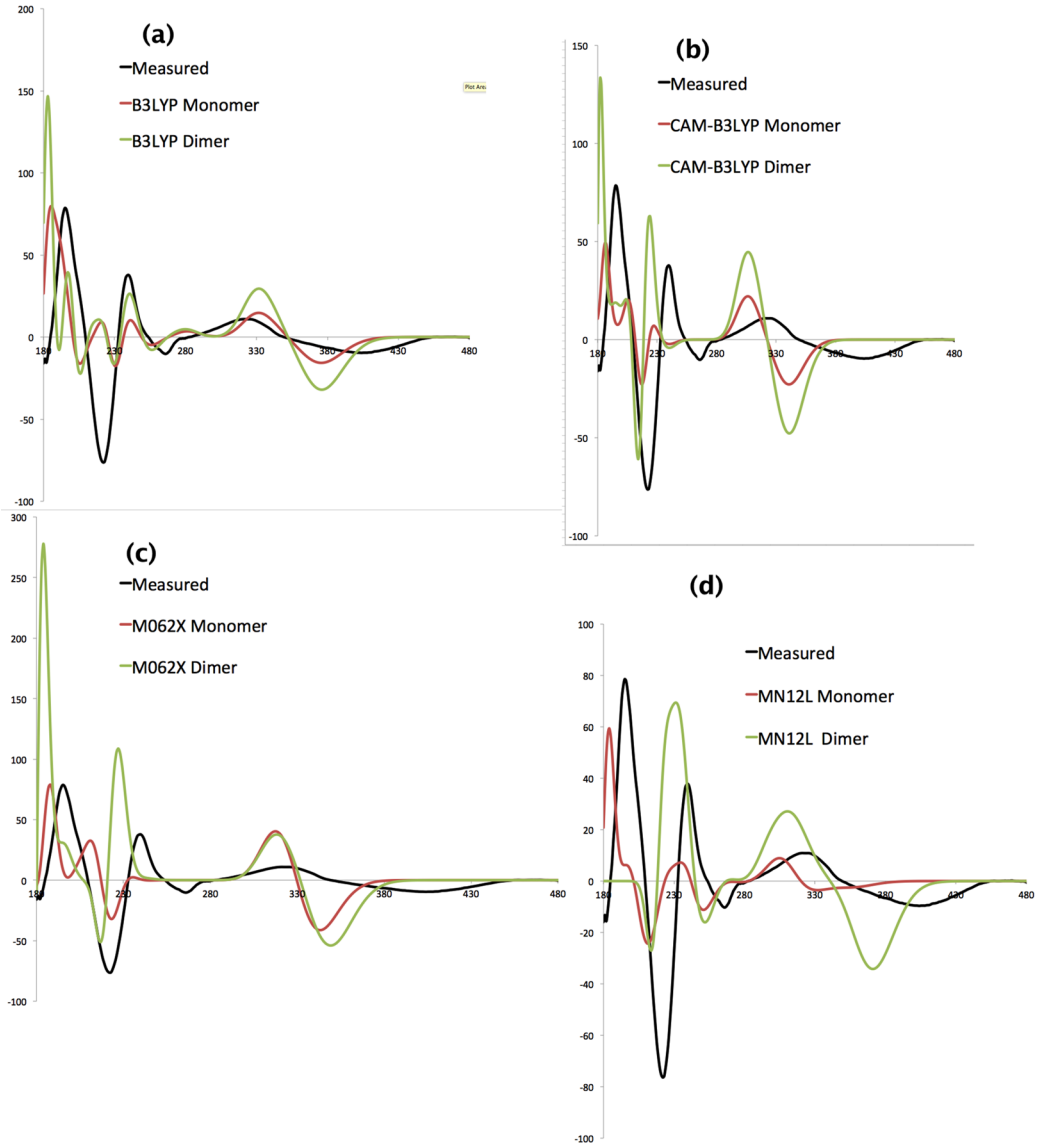

Figure 6. Calculated ECD spectra of (−)-brevianamide B with a continuum solvent field (SCRF/TFE) for both monomer **3** and dimer **4** using the 6-311++G(d,p) basis set and the functionals (a) B3LYP, (b) CAM-B3LYP, (c) M052X, and (d) MN12L. The calculated ECD curves were unshifted and convoluted with a line width of 0.15 eV. The normalized experimental data (Figure 1), measured in TFE, are overlaid for comparison (black curve). Individual traces can be accessed via the spreadsheet provided for this figure with the Supporting Information.

like dimerization. In the case of carboxylic acids, the effects of dimerization are usually observed in the CO stretch region. By the study of the changes in spectrum upon changing the concentration of the acids involved, it is possible to determine the stability of such dimers. To shed more light on the results obtained with ECD, we set out to obtain a VCD spectrum of our brevianamide B sample in solution. VCD has the advantage of being based on vibrational transitions, of which there are potentially many more than resolvable electronic transitions. The resulting spectra are therefore potentially richer in information. However, recording the required VCD spectrum was technically challenging. The low quantities of material we had access to (<1 mg), the low solubility of brevianamide B, and the low absorption intensity of VCD modes of absorption limited the utility of conventional VCD methods. The solubility in trifluoroethanol was sufficient to allow a specific robust carbonyl stretch feature in the VCD spectrum to be used, although this unfortunately prevented the use of the OH stretching region. All other bands are much weaker and were not observed.

The experimental IR and VCD spectra for brevianamide B dissolved in TFE-d_3 are shown in Figure 8A,B. The calculated IR and VCD spectra for the monomer and dimer are given in Figure 8C−F. In the experimental IR spectra, a broad, intense feature and a weaker shoulder is observed near 1675 and 1620 cm^{-1}. Based on visual inspection of the normal modes involved, the former is assigned to combinations of the three C═O stretching modes, which in the monomer are predicted to occur near 1774, 1767, and 1756 cm^{-1}. The latter are assigned to two nearly degenerate skeletal deformations in the indoxil substructure. Despite the low sample concentration and the fact that the intensity of the carbonyl stretching modes in the IR hardly exceeds 0.15 absorbance units, a split-type bisignate CD signal is observed in the VCD spectrum. The exact nature of this CD signal observed is directly related to the mixing of the C═O stretching modes in the different carbonyl IR

DOI: 10.1021/jo5022647
J. Org. Chem. 2015, 80, 3359−3367

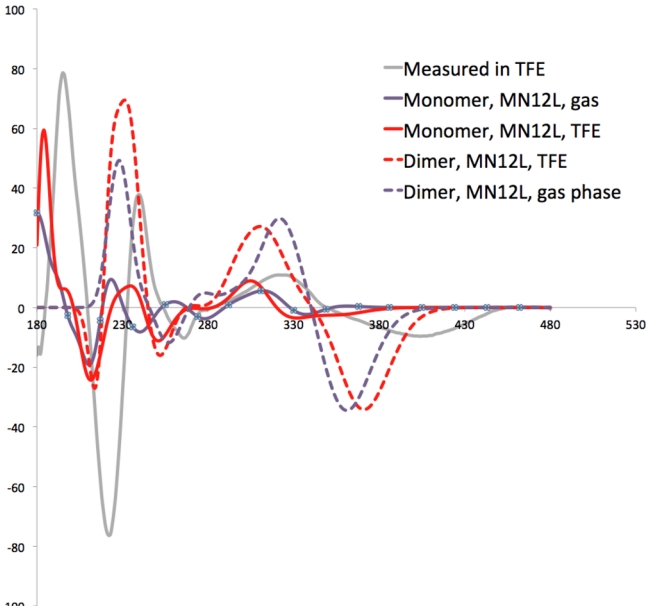

Figure 7. Calculated ECD spectra of (−)-brevianamide B for both monomer **3** and dimer **4** using the 6-311++G(d,p) basis and the MN12L functional, for both gas phase and TFE solution. The calculated ECD curves were unshifted and convoluted with a line width of 0.15 eV.

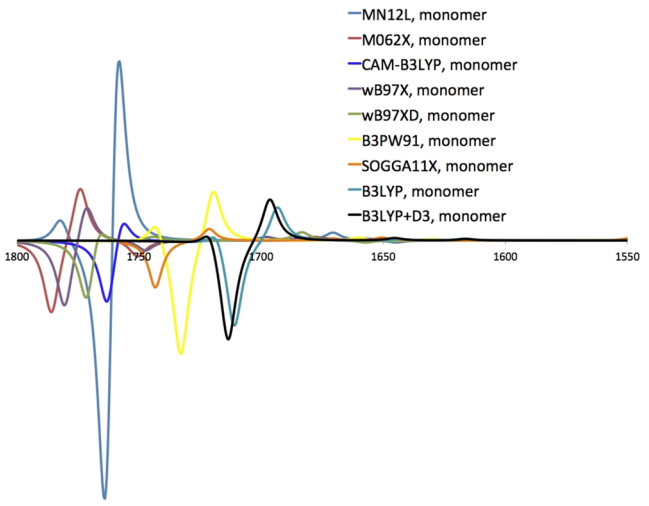

Figure 9. VCD spectra for monomer **3** obtained for a range of functionals using 6-311++G(d,p) scrf(cpcm, solvent=TFE) over the region of 1550−1800 cm^{-1}. Individual traces can be accessed via the spreadsheet provided for this figure with the Supporting Information.

chromophores present. Comparison of calculated and experimental VCD data, however, should enable analysis of the absolute configuration of the sample and also be able to discriminate between monomer **3** and dimer **4**.

Figure 8 reveals that, in solution, the monomer simulation using the MN12L functional fits experiment qualitatively better than that of the dimer. At the suggestion of a referee that we might still be confronted with a fortuitously good agreement for the functional chosen and in light of the sensitivity of the

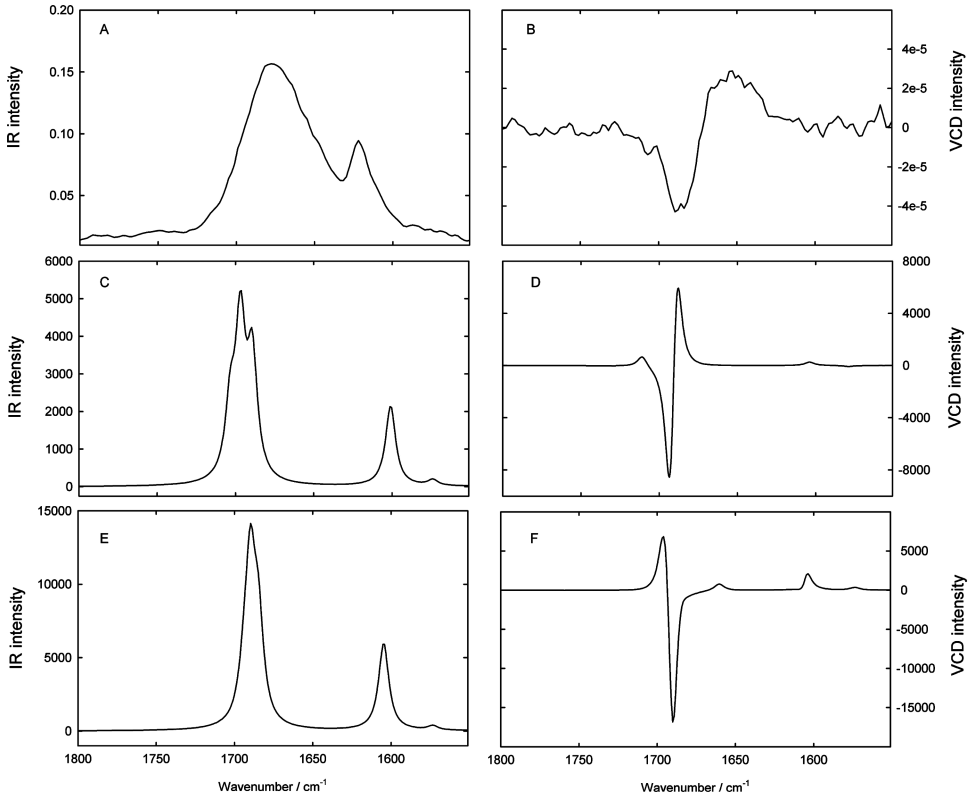

Figure 8. IR and VCD spectra of (−)-brevianamide B. Panels A and B show the experimental IR and VCD spectra for brevianamide B obtained for a solution in TFE-d_3 over the range of 1550−1800 cm^{-1}. Panels C and D show the calculated IR and VCD spectra obtained at the MN12L/6-311++G(d,p) scrf(cpcm, solvent=TFE) level for monomer **3**. Panels E and F show the calculated IR and VCD spectra obtained at MN12L/6-311++G(d,p) scrf(cpcm, solvent=TFE) for dimer **4**. The theoretical spectra were obtained by using a scale factor of 0.960.

DOI: 10.1021/jo5022647
J. Org. Chem. 2015, 80, 3359−3367

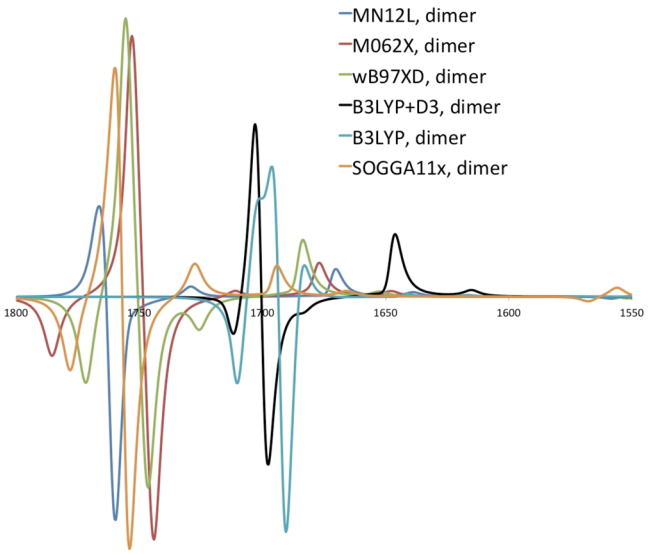

Figure 10. VCD spectra for dimer **4** obtained for a range of functionals using 6-311++G(d,p) scrf(cpcm, solvent=TFE) over the region of 1550−1800 cm^{-1}. Individual traces can be accessed via the spreadsheet provided for this figure with the Supporting Information.

simulated ECD data to the functional employed, we surveyed a range of functionals for VCD prediction in the carbonyl stretching region for both monomer **3** (Figure 9) and dimer **4** of brevianamide B (Figure 10).

The negative and positive observed Cotton effects for the high and low wavenumber components of the bisignate CD carbonyl stretching signal are reproduced by all functionals considered for the monomer simulation (Figure 9). Likewise, all tested methods predict more complex but essentially inverse Cotton effect behavior for this signal for dimer **4** (Figure 10). The uniformity of the Cotton effect behavior over all functionals establishes the robustness of the carbonyl stretch region. Thus, we can unambiguously conclude from the comparison of the experimental VCD spectrum with the predicted ones that the monomeric species **3** in TFE solution is the predominant molecular form in dilute solution. More generally, because of the large functional dependence of ECD spectra and the more robust nature of VCD spectra over the range of different functionals used, we recommend that VCD is a better technique for also establishing the absolute configuration of such molecules. Our work supports the absolute stereochemical assignment of this compound, originally established using total synthesis.[12]

CONCLUSIONS

We have generated high-quality ECD and VCD data to enable a chiroptical study on brevianamide B (**3**). We have found the simulation of brevianamide B ECD data to be subtly dependent on the functional employed. The relatively poor agreement between the experimental and simulated data using the M062X functional led us to investigate the suggestion of a hydrogen-bonded molecular dimer. Through free energy calculations, ECD simulations with the MN12L functional, and particularly, comparative VCD studies, ultimately this hypothesis proved incorrect, with the solution chiroptical spectra obtained representing a single monomeric species. VCD is found to be a more reliable technique in the sense that the computationally obtained reference spectra are more robust, depending significantly less on the details of the calculations than is the case for ECD spectra.

It remains to be determined as to whether our proposed dimeric structure for brevianamide B (**4**, Figure 4b) would be observed in the solid state. Although an X-ray crystallographic structure of a brevianamide B analogue has been solved,[8a] the crystallized analogue bears a *para*-methoxybenzyl group on the diketopiperazine nitrogen atom ("N3" in Figure 4) that would disrupt the proposed hydrogen-bond network. We note that there is ample precedence from 376 other known crystal structures of the bifurcated hydrogen-bonding network in our dimer model. It is perhaps telling that, unlike brevianamide A, brevianamide B is extremely insoluble in the majority of solvents examined, as also noted by Birch and co-workers in their original isolation study.[10b]

EXPERIMENTAL SECTION

General. The sample of brevianamide B employed was prepared from (+)-brevianamide A (see Scheme 1) using previously reported methods.[10]

Computational Procedures. *Conformation:* All the rings present in **3** are conformationally locked except for the terminal 5-ring, which has two possible conformations that have a predicted Boltzmann population ranging from ∼69/31% in favor of conformer **3**(**1**) to a more equal population depending on the functional and basis set used. Conformation **3**(**1**) was used for the simulations reported here because the differences predicted for conformation **3**(**2**) are small and localized, as noted below.

Electronic Circular Dichroism: TDDFT calculations using the basis sets and functionals stated with a continuum solvent model for up to 250 states were used to simulate the electronic circular dichroism spectra. Comparison of ECD spectra for the conformational form **3**(**1**) and **3**(**2**) indicates the only perceptible differences are a ∼5 nm blue shift for **3**(**2**) in the region of 230 nm and some small intensity differences. Some functional combinations (e.g., B3LYP+D3) did not converge even for 150 states for the dimer species and are therefore not included in the comparisons.

Vibrational Circular Dichroism: Spectra were also computed using the basis sets and functionals stated with a continuum solvent model using the standard methods implemented in Gaussian 09, with the addition of the keyword integral=(acc2e=12,grid=ultrafine) required to ensure convergence of the first-order CPHF calculation. Only small VCD intensity differences between conformations **3**(**1**) and **3**(**2**) were detected in the 1600−1800 cm^{-1} window selected; the phases of the Cotton effects for these signals were the same for both conformations. Further details can be found in the Supporting Information, as can all the input parameters and resulting outputs from the calculations via the Web-enhanced-object (WEO1) and links therein to the digital repository entries for each calculation.

Chiroptical Measurements. *ECD Spectroscopy:* The experimental ECD spectra were recorded using the synchrotron CD beamline at the Diamond Light Source, UK.

VCD Measurements: Experimental IR and VCD spectra were measured at the European Centre for Chirality (EC^2) in Belgium on a BioTools ChiralIR-2X instrument using a solution of (−)-brevianamide B TFE-d_3. All spectra were recorded using a demountable liquid cell equipped with BaF_2 windows and 100 μm spacers. All spectra were recorded at 4 cm^{-1} resolution for approximately 13 h, accumulating 40 000 scans. The spectra shown were obtained using a solution of 1.2 mg of brevianamide B dissolved in 0.135 mL of TFE-d_3. Background corrections for VCD were introduced by subtracting the spectrum obtained for pure TFE-d_3.

ASSOCIATED CONTENT

Supporting Information

Simulated ECD and VCD spectra are available in spreadsheet form (.xlsx) for Figures 3, 6, 7, 9, and 10. A selection of

DOI: 10.1021/jo5022647
J. Org. Chem. 2015, 80, 3359−3367

measured crystal structures bearing the intermolecular bifurcated hydrogen-bond motif revealed in Figure 4b is available as a multistructure CIF file. The UV−vis spectra of brevianamide A and B. This material is available free of charge via the Internet at http://pubs.acs.org.

AUTHOR INFORMATION

Corresponding Authors

*E-mail: m.fuchter@imperial.ac.uk.

*E-mail: rzepa@imperial.ac.uk.

Notes

The authors declare no competing financial interest.

ACKNOWLEDGMENTS

We would like to thank Professor Robert Williams for the kind provision of the brevianamide sample. We acknowledge Diamond Light Source for time on B23 under proposal SM7994. We thank Emiliana DeSantis for additional support with ECD measurements. P.B. and W.H. acknowledge the Flemish Fund for Scientific Research (FWO Vlaanderen) and the BOF/IOF funding agencies at Antwerp and Ghent University for continuous support. The computational resources (Stevin Supercomputer Infrastructure) and services used in part of this work were provided by the VSC (Flemish Supercomputer Center), funded by Ghent University and the University of Antwerp, the Hercules Foundation, and the Flemish Government—Department EWI.

REFERENCES

(1) Eliel, E. L.; Wilen, S. H *Stereochemistry of Organic Compounds*; John Wiley & Sons: New York, 1994.

(2) Barron, L. D.; Buckingham, A. D. *Chem. Phys. Lett.* **2010**, *492*, 199−213.

(3) Mukhopadhyay, P.; Wipf, P.; Beratan, D. N. *Acc. Chem. Res.* **2009**, *42*, 809−819.

(4) Polavarapu, P. L. *Chirality* **2008**, *20*, 664−672.

(5) Cherblanc, F.; Lo, Y.-P.; De Gussem, E.; Alcazar-Fuoli, L.; Bignell, E.; He, Y.; Chapman-Rothe, N.; Bultinck, P.; Herrebout, W. A.; Brown, R.; Rzepa, H. S.; Fuchter, M. J. *Chem.—Eur. J.* **2011**, *17*, 11868−11875.

(6) Cherblanc, F. L.; Lo, Y.-P.; Herrebout, W.; Bultinck, P.; Rzepa, H. S.; Fuchter, M. J. *J. Org. Chem.* **2013**, *78*, 11646−11655.

(7) Berova, N.; Di Bari, L.; Pescitelli, G. *Chem. Soc. Rev.* **2007**, *36*, 914−931.

(8) (a) Williams, R. M.; Glinka, T.; Kwast, E.; Coffman, H.; Stille, J. K. *J. Am. Chem. Soc.* **1990**, *112*, 808−821. (b) Williams, R. M.; Sanz-Cervera, J. F.; Sancenon, F.; Marco, J. A.; Halligan, K. *J. Am. Chem. Soc.* **1998**, *120*, 1090−1091. (c) Williams, R. M.; Sanz-Cervera, J. F.; Sancenón, F.; Marco, J. A.; Halligan, K. *Bioorg. Med. Chem.* **1998**, *6*, 1233−1241. (d) Williams, R. M.; Cox, R. J. *Acc. Chem. Res.* **2003**, *36*, 127−139. (e) Adams, L. A.; Valentea, M. V. N.; Williams, R. M. *Tetrahedron* **2006**, *62*, 5195−5200. (f) Frebault, F. C.; Simpkins, N. S. *Tetrahedron* **2010**, *66*, 6585−6596.

(9) Birch, A. J.; Wright, J. J. *J. Chem. Soc., Chem. Commun.* **1969**, 644−645.

(10) (a) Birch, A. J.; Wright, J. J. *Tetrahedron* **1970**, *26*, 2329−2344. (b) Birch, A. J.; Russell, R. A. *Tetrahedron* **1972**, *28*, 2999−3008. (c) For a recent review that includes isolation of brevianamides M, S, and T-V, see Blunt, J. W.; Copp, B. R.; Keyzers, R. A.; Munroa, M. H. G.; Prinsep, M. R. *Nat. Prod. Rep.* **2014**, *31*, 160−258. (d) For a recent study on brevianamide M that includes a chiroptical study, see Ren, J.; Li, G.-Y.; Shen, L.; Zhang, G.-L.; Nafie, L. A.; Zhu, H.-J. *Tetrahedron* **2013**, *69*, 10351−10356.

(11) Coetzer, J. *Acta Crystallogr.* **1974**, *B30*, 2254−2256.

(12) Williams, R. M.; Glinka, T.; Kwast, E. *J. Am. Chem. Soc.* **1988**, *110*, 5927−5929.

(13) Williams, R. M.; Kwast, E.; Coffman, H.; Glinka, T. *J. Am. Chem. Soc.* **1989**, *111*, 3064−3065.

(14) Asai, T.; Taniguchi, T.; Yamamoto, T.; Monde, K.; Oshima, Y. *Org. Lett.* **2013**, *15*, 4320−4323.

(15) Frisch, M. J.; Trucks, G. W.; Schlegel, H. B.; Scuseria, G. E.; Robb, M. A.; Cheeseman, J. R.; Scalmani, G.; Barone, V.; Mennucci, B.; Petersson, G. A.; Nakatsuji, H.; Caricato, M.; Li, X.; Hratchian, H. P.; Izmaylov, A. F.; Bloino, J.; Zheng, G.; Sonnenberg, J. L.; Hada, M.; Ehara, M.; Toyota, K.; Fukuda, R.; Hasegawa, J.; Ishida, M.; Nakajima, T.; Honda, Y.; Kitao, O.; Nakai, H.; Vreven, T.; Montgomery, J. A., Jr.; Peralta, J. E.; Ogliaro, F.; Bearpark, M.; Heyd, J. J.; Brothers, E.; Kudin, K. N.; Staroverov, V. N.; Kobayashi, R.; Normand, J.; Raghavachari, K.; Rendell, A.; Burant, J. C.; Iyengar, S. S.; Tomasi, J.; Cossi, M.; Rega, N.; Millam, M. J.; Klene, M.; Knox, J. E.; Cross, J. B.; Bakken, V.; Adamo, C.; Jaramillo, J.; Gomperts, R.; Stratmann, R. E.; Yazyev, O.; Austin, A. J.; Cammi, R.; Pomelli, C.; Ochterski, J. W.; Martin, R. L.; Morokuma, K.; Zakrzewski, V. G.; Voth, G. A.; Salvador, P.; Dannenberg, J. J.; Dapprich, S.; Daniels, A. D.; Farkas, Ö.; Foresman, J. B.; Ortiz, J. V.; Cioslowski, J.; Fox, D. J. *Gaussian 09*, revision D.01; Gaussian, Inc.: Wallingford, CT, 2009.

(16) (a) Autschbach, J. *Chirality* **2009**, *21*, E116−E152. (b) Di Bari, L.; Pescitelli, G. Electronic Circular Dichroism. In *Computational Spectroscopy - Methods, Experiments and Applications*; Grunenberg, J., Ed.; Wiley-VCH: Weinheim, Germany, 2010; pp 241−272.

(17) Grimme, S.; Antony, J.; Ehrlich, S.; Krieg, H. *J. Chem. Phys.* **2010**, *132*, 154104.

(18) Allen, F. H. *Acta Crystallogr.* **2002**, *B58*, 380−388.

(19) (a) Cappelli, C.; Corni, S.; Mennucci, B.; Cammi, R.; Tomasi, J. *J. Phys. Chem. A* **2002**, *106*, 12331−12339. (b) Wang, F.; Polavarapu, P. L. *J. Phys. Chem. A* **2000**, *104*, 10683−10687. (c) He, J. T.; Polavarapu, P. L. *J. Chem. Theory Comput.* **2005**, *1*, 506−514. (d) Urbanova, M.; Setnicka, V.; Devlin, F. J.; Stephens, P. J. *J. Am. Chem. Soc.* **2005**, *127*, 6700−6711. (e) Kuppens, T.; Herrebout, W.; Van Der Veken, B.; Bultinck, P. *J. Phys. Chem. A* **2006**, *110*, 10191−10200. (f) Yang, G.; Xu, Y. *Phys. Chem. Chem. Phys.* **2008**, *10*, 6787−6795. (g) Góbi, S.; Vass, E.; Magyarfalvi, G.; Tarczay, G. *Phys. Chem. Chem. Phys.* **2011**, *13*, 13972−13984.

DOI: 10.1021/jo5022647
J. Org. Chem. 2015, 80, 3359−3367